Simple qualitative dynein model in Nose-Hoover framework

J. Rosenberg[a,*], M. Krejčová[a]

[a]*NTIS – New Technologies for the Information Society, Faculty of Applied Sciences, University of West Bohemia, Technická 8, Pilsen, Czech Republic*

Abstract

The presented paper is devoted to studying the dynein molecular motor and its stochastic description. The model aims to obtain good results comparable to literature sources qualitatively. We choose the Hoover-Holian oscillator to describe the dynein behaviour of each of its legs. It can catch the stochastic movement produced by Brownian motion and can be modified to simulate a load.
ⓒ 2022 University of West Bohemia.

Keywords: dynein, Hoover-Holian oscillator, catch bond effect

1. Introduction

Dynein seems to be one of the essential processive molecular motors. Its structure and motion are very different compared to other processive molecular motors, like kinesin or myosin V. According to the current knowledge, it is connected with neurodegenerative diseases like Parkinson's, Alzheimer and ALS [9]. Also, it has an essential role in glaucoma [6]. Maybe the most interesting part is the role of dynein in viral infection [11,29]. Dyneins can be very diverse in their structure. It is possible to say that a whole family of dynein motors exists. The main difference is in their number of heads, see Fig. 1. The cytoplasmic dynein has two heads. Here, we will focus on this type.
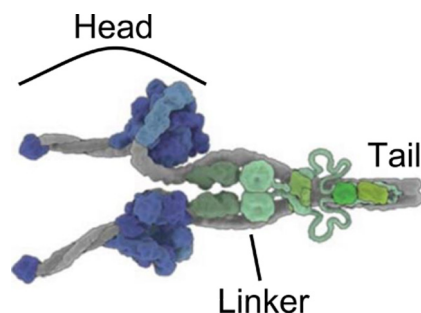

Fig. 1. Scheme of cytoplasmic dynein – a single tail connects two heads, adapted from [7]

A more detailed scheme of a cytoplasmic dynein head is in Fig. 2. The stalk can be bound to the microtubule via electrostatic force [19] to the microtubule-binding domain (MTBD). Six subunits of AAA+ ATPase create the most significant part of the head (the motor domain). The linker connects the motor domain with the tail.

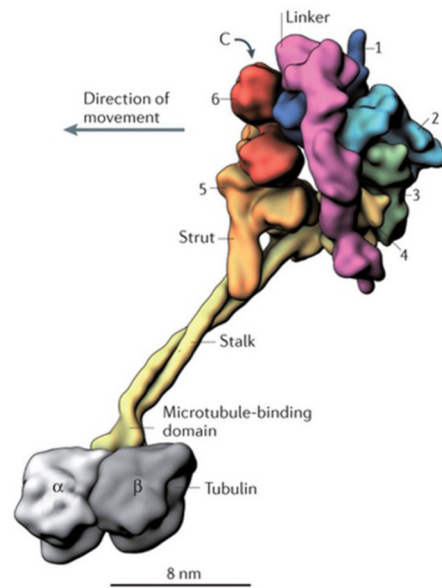*Corresponding author. Tel.: +420 377 632 325, e-mail: rosen@kme.zcu.cz.

Fig. 2. Detail scheme cytoplasmic dynein – its one head, the numbers label six subunits of AAA+ ATPase, adapted from [28]
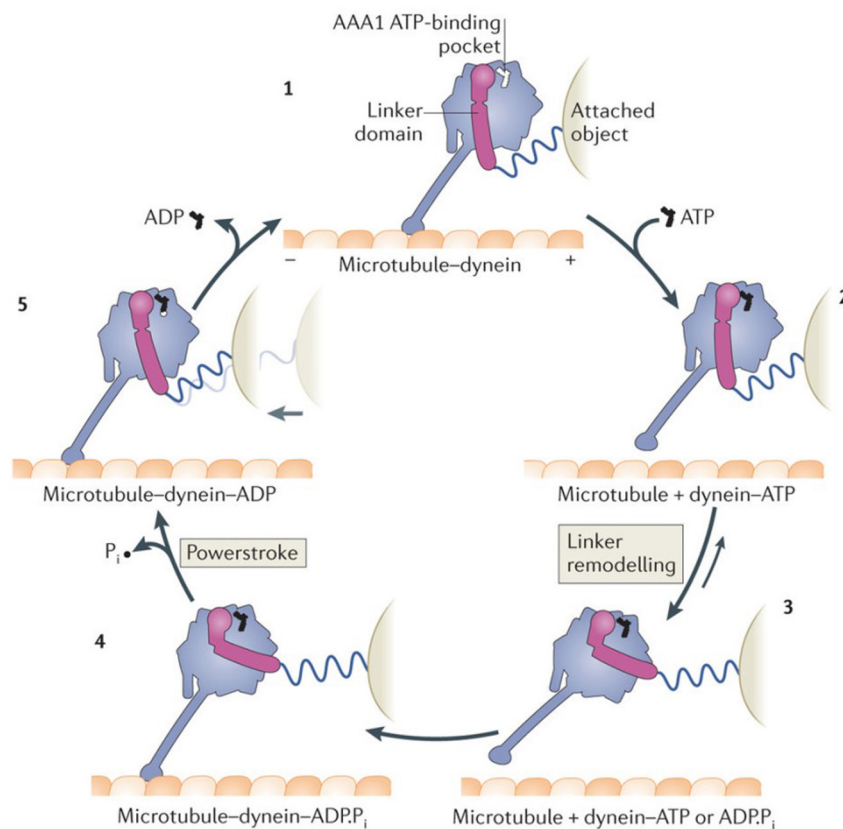

Fig. 3. The working cycle of cytoplasmic dynein, adapted from [28]

The mechanochemical dynein cycle is according to [3] as follows, Fig. 3: Concurrently, the linker crosses the AAA+ ring doing the priming stroke. This stroke moves the stalk and MTBD towards the minus ($-$) end of the microtubule (MT). After the adenosine triphosphate molecule (ATP) hydrolysis, the head binds to MT again. However, in a new position. The inorganic phosphate is released, and the linker returns to the starting unprimed state – it does the power

stroke. The head is moving ahead. In this phase, the molecular motor produces mechanical work. The cycle can be described differently, for example, like in [28], see Fig. 3.

That is the description of the mechanochemical cycle of one motor domain. As was mentioned above, the whole cytoplasmic dynein motor consists of these two domains and can perform continuous motion along the microtubule. This motor is processive because one stalk bounds to the MT always. During this motion, it can bring the cargo from the (+) end of MT (e.g., membrane) to the (−) end (e.g., nucleus). The cargoes can be different organelles or even viruses.

For this purpose, both heads have to be coordinated or at least in some relation. This point is now-a-day not sufficiently discovered. Another open problem is the behaviour of the dynein under acting force.

Dynein properties and its differences from other processive molecular motors kinesin and myosin V are summarised in the review [4]:

- Both motor domains operate largely independently during the motion. They are moving parallel on the two "trails" of MT. Kinesin and myosin V reveal the hand-over-hand movement. The rear head always passes the front head. On the contrary, in the case of dynein, the rear or front head can take steps/steps without passing another head. Also, the order of heads stepping seems to be stochastic one head can do one, two or even three steps before another head moves. With the growing distance between both heads, the probability of the forward stepping off the front head decreases and the front head can move backwards, or the rear head can move forward.

- In general, we can distinguish four different types of steps [25], which are observable in Fig. 4:

    - alternating and passing steps ("hand-over-hand" – light green and red asterisks),
    - alternating and not passing steps ("inchworm" – dark green and red asterisks),
    - not alternating and passing steps (light green and light orange asterisks),
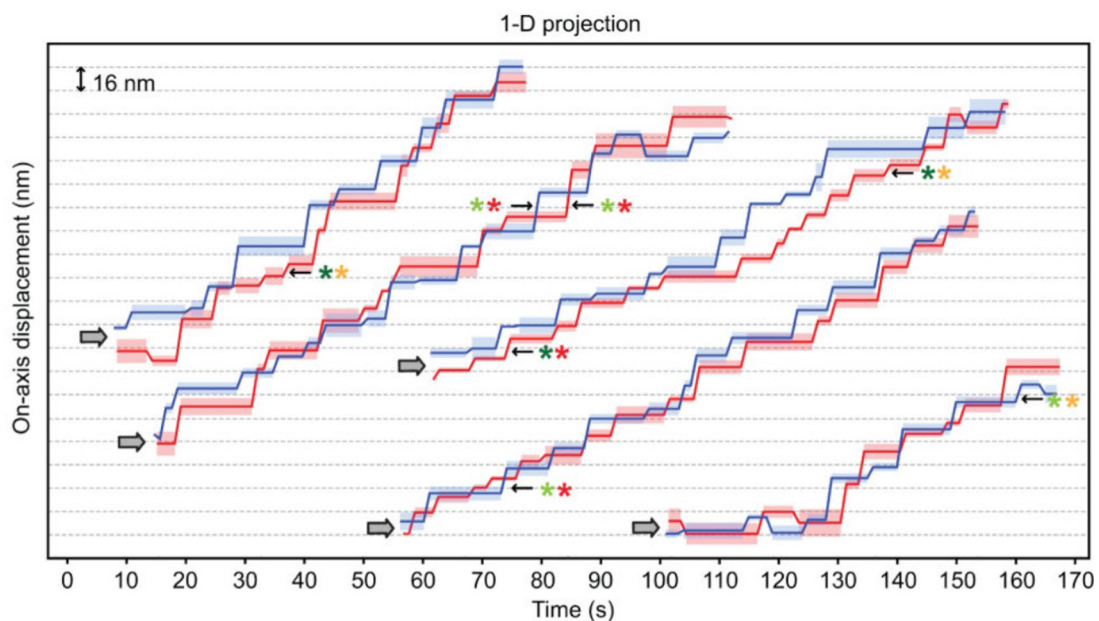   - not alternating and not passing steps (dark green and light orange asterisks).

Fig. 4. Steps variants of cytoplasmic dynein (the meaning of stars is explained in the text above), adapted from [25]

- Under zero load, dynein takes in 20% of the time backward steps. The size of the steps varies between 8 and 32 nm.

- Forward stepping is preferred. Only higher tension between both motor domains can cause backwards stepping.

- The motion of one stalk during the step can be divided into two phases: First, the MTBD is bound weakly to the MT. Then, under Brownian search, MTBD is located in another binding place (forwards or backwards) where the binding force is strong.

- Another essential property of dynein is the change of the step length. With increasing force, the step length decreases. Different sites on the AAA ring control this property, see Fig. 2. The site controlling the smallest length is working with different kinetics that mimics the "catch-bond" behaviour [17, 18, 20, 24, 26, 30]. This site's catalysis rate increases with the increasing load, while its ATP binding rate (causing the detachment) decreases.

- The velocity of dynein can be very different. For human dynein, the authors of [5] mention the unloaded velocity and the stall force to be $v = 540 \pm 60$ nm/s and $Fs = 1.9 \pm 0.2$ pN, respectively. Similar values can be found, e.g., in [1].

- In [4], it is stressed that there are many unknowns about the dynein.

- It should be mentioned that dynein can also provide the sideways steps. It can switch the lines on the microfilament, see, e.g., [21, 27, 33]. Then, the motion is described as a 2D problem.

Another important issue is the binding of different cargoes with dynein. For this purpose, other proteins are necessary, e.g., dynactin bound with dynein creates one complex [8], Fig. 5.
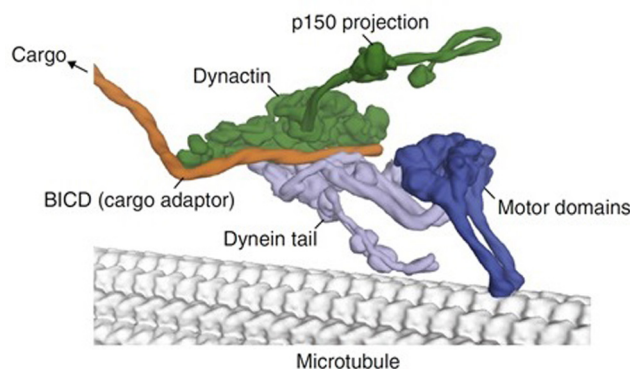

Fig. 5. Dynein structure, adapted from [8]

There are some computer models of dynein such as the pure deterministic model [12], the stochastic model [13] or the very simple model [35], which omits, e.g., the backwards possibility. Goedecke's model [13] is very complicated and based on the Langevin equation for the simulation of the diffusion motion. The very sophisticated model was recently published in [32]. It is based on the Crossley's model [12], but it is enormously improved. It already allows us to simulate the influence of different mutations like Legs at odd angles (Loa), Cramping 1 (Cra1), Sprawling (Swl) and others. A very detailed description of the model is in [31].

We aim to develop a relatively simple model that considers the complicated structure of dynein, all the phases of steps and the diffusion motion of the stalks and cargo. The Nose-Hoover oscillator simulates the Brownian motion. This approach is described in the following sections. This model should simulate the mutations and the influence of different drugs such as Dynarrestin or alcohol.

2. Brownian motion and Nose-Hoover oscillator

In [15], the authors stress at the beginning the possibility to simulate the "stochastic" and "Brownian" dynamics using a deterministic time-reversible thermostat. The deterministic system of ordinary differential equations with only a few degrees of freedom replaces the commonly used stochastic Langevin equation. The detailed description of these models is not in the scope of this contribution and can be found in the papers mentioned below. The development of these systems started with the thermodynamic description in [15]. It was improved in the follow up papers by Hoover and his co-workers. The reason for all these improvements was to enhance the ergodicity. The original 3D Nose-Hoover oscillator was not fully ergodic, and the best solution was to add a variable. These 4D oscillators are also less stiff and easier to solve.

In [15], seven different models are mentioned. In the later work [16], Hoover et al. introduced the latest three models. The ergodicity is proven in the case of the Hoover and Holian oscillator (HH oscillator)

$$\frac{\mathrm{d}x}{\mathrm{d}t} = p, \tag{1}$$

$$\frac{\mathrm{d}p}{\mathrm{d}t} = -x - \zeta p - \xi p^3, \tag{2}$$

$$\frac{\mathrm{d}\zeta}{\mathrm{d}t} = p^2 - 1, \tag{3}$$

$$\frac{\mathrm{d}\xi}{\mathrm{d}t} = p^4 - 3p^2. \tag{4}$$

In comparison with the original Nose-Hoover oscillator (equations (14) in [23]), here is the fourth variable ξ. The results are shown in Fig. 6.
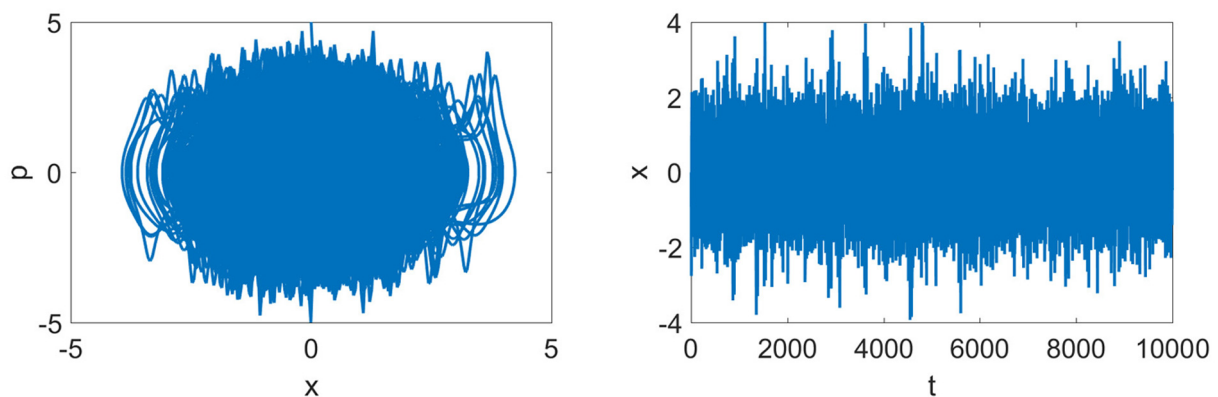

Fig. 6. Examples of Hoover and Holian oscillator chaotic behaviour

Using the algorithm published in [34], the Lyapunov exponents of the analysed HH oscillator were calculated, Fig. 7. If we start from the arbitrary point in the neighbourhood of the attractor, the spectrum of Lyapunov exponents is the same and has approximately the form $(+, 0, -)$. Another important graph displaying the property of the HH oscillator is the histogram of the samples taken within the different time-period ff. We used the MATLAB function `histfit`. This function uses the number of bins equal to the square root of the number of elements in the data and then superimposes a fitted normal distribution, see Fig. 8.
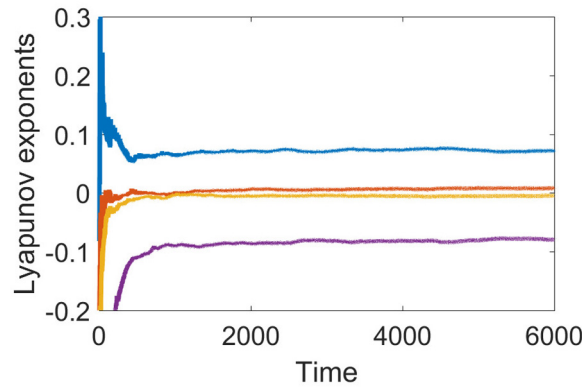
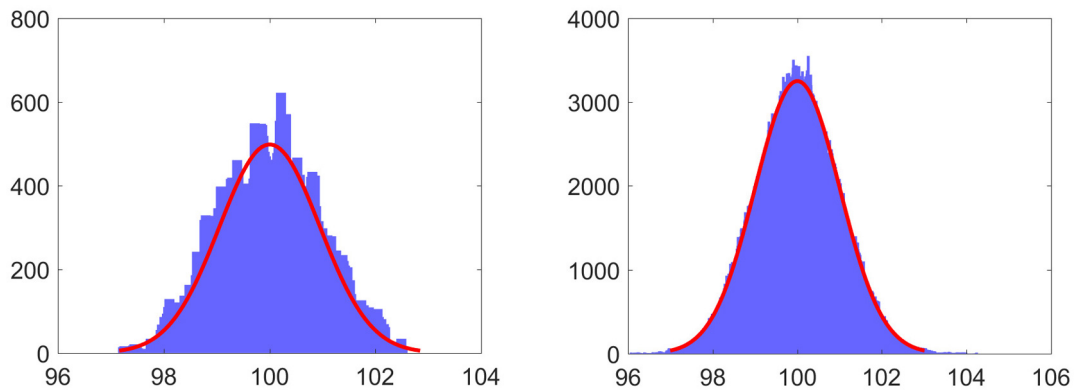Fig. 7. Lyapunov exponents of Hoover and Holian oscillator

Fig. 8. Histogram of samples with given period ff given by the Hoover and Holian oscillator. The left figure is for fewer samples than the right one. Both show that the distribution converges to a Gaussian one

3. Mathematical model of dynein

At first, we consider only one motor domain (in a further text called motor only). We solve its motion in 1D space. The sideways steps are not taken into account. It seems to be appropriate to use the 1D state chemically driven flashing ratchets in the model [2, 14, 22]. Later on, the number of states can be higher. The motor position on the polar and periodic track, in the case of dynein microtubulin (MT), is given by the coordinate x. The interaction between motor and MT is described with the potentials $W_i(x)$ depending on the motor state i, $i = 1, 2$. A chemical reaction triggers the transition between both states. Here, ATP and its hydrolysis. In the following text, the model is described omitting the details. The reason for this omission is to show the basic scheme. All used model parameters and their meaning is summarised in Table 1. For abbreviations, see Table 2.

Table 1. List of model parameters

L	potential period
$delta$	limit of boundaries of the domains distance (measure of the domain dependence)
ni	frequency of the steps
ff	sampling period
kk	parameter influencing the length of the Brownian motion
$Fload$	external load
sc	width of the HH attractor
rat	position of the potential minimum
$invstif$	1/stiffness of the one domain
ps	power stroke
$deltacb$	catch bond parameter (see Fig. 14)
cb	catch bond parameter (see Fig. 14)
$kkcb$	value of kk in the case of catch bond
$nicb$	value of ni in the case of catch bond

Table 2. List of abbreviations

ALS	amyotrophic lateral sclerosis
ATP	adenosine triphosphate
HH, PB, MKT	choice of the oscillator type (Hoover-Holian, Patra Bhattacharya, Martyna-Klein-Tuckerman)
MT	microtubulus
MTBD	microtubulus biding domain
ODE	ordinary differential equation

3.1. Deterministical model of the dynein

While we try to model the dynein with the deterministic dynamical system, another approach will be used. The cargo will not be taken into account. The Brownian motion during this phase, where the stalk detaches from MT caused by ATP (left green arrow in Fig. 9), is modelled with the Nose-Hoover oscillator. After hydrolysis of ATP, the potential W causes the strong binding of the MTBD with MT (right green arrow). The place of this binding position is in the minimum of the potential W (red arrow). The choice of this minimum depends on the MTBD current position and the last position of the Nose-Hoover oscillator. If the interval of its attractor is large enough, it can be one, two or even more periods forward or backwards.

The potential has the simple form

$$W = U_0 \left(\sin \frac{2\pi}{L} x + \frac{1}{2} \sin \frac{4\pi}{L} x + \frac{1}{3} \sin \frac{2\pi}{L} x \right), \tag{5}$$

where L is the period of this periodical and unsymmetric potential and x is the position on MT. Fig. 10a shows the graph of this function for $L = 8\,\text{nm}$ and $U_0 = 26.7\,\text{k}_\text{B}\text{T}$. Involving the external force corresponds with the producing a slope along with both potentials, see Fig. 10b. In Fig. 9 and in the following figures, the graph of potential is only simplified drawn.
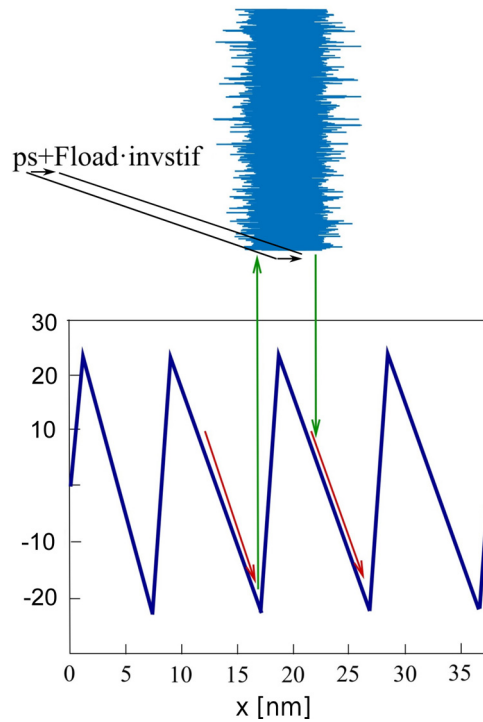
Fig. 9. Brownian motion described by the Nose-Hoover oscillator with the potential given by the usual form $W = U_0 \left(\sin \frac{2\pi}{L} x + \frac{1}{4} \sin \frac{4\pi}{L} x \right)$. In this and the other figures below, the potential is graphically simplified. The coil represents the chaotic motion of the stalk
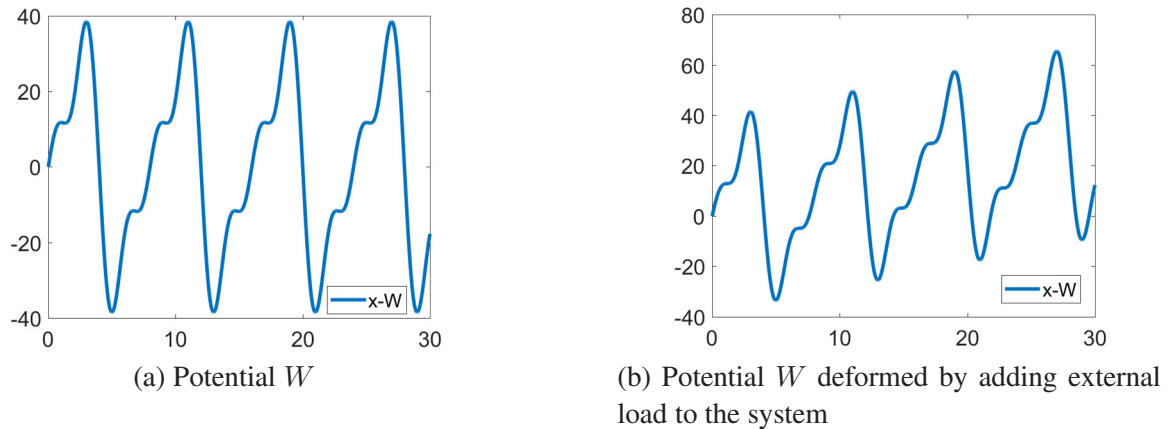

(a) Potential W

(b) Potential W deformed by adding external load to the system

Fig. 10. Asymmetrical potentials

The equations describing the Brownian motion are a little bit more complicated to allow simulation not only of the Hoover-Holian oscillator but also the others described [16]. These oscillators are called Martyna-Klein-Tuckerman (MKT) and Patra-Bhattacharya (PB) oscillators

$$\frac{\mathrm{d}x}{\mathrm{d}t} = p - PB\xi x, \tag{6}$$

$$\frac{\mathrm{d}p}{\mathrm{d}t} = -p\zeta - x - HH\xi p^3, \tag{7}$$

$$\frac{\mathrm{d}\xi}{\mathrm{d}t} = (p^4 - 3p^2)HH + MKT(\zeta^2 - 1) + PB(x^2 - 1), \tag{8}$$

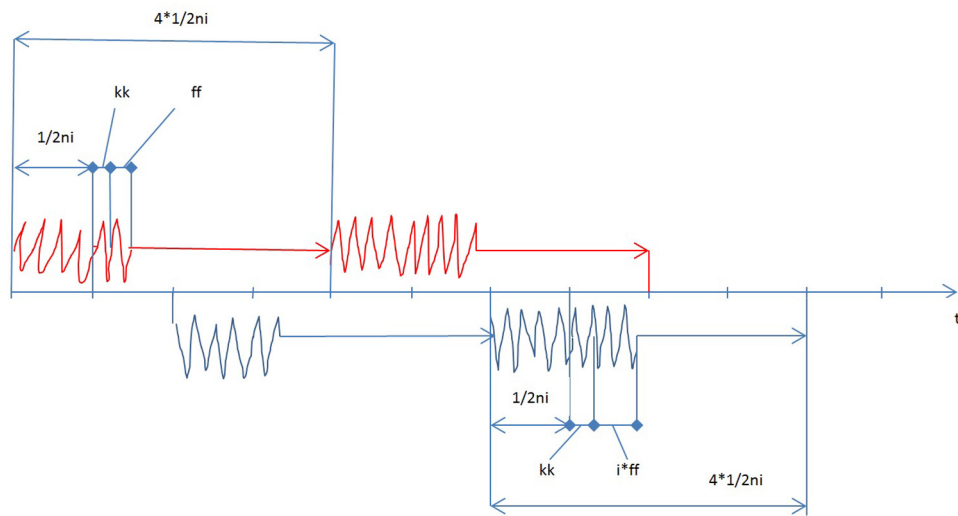$$\frac{\mathrm{d}\zeta}{\mathrm{d}t} = (p^2 - 1)\alpha - MKT\xi\zeta. \tag{9}$$

Fig. 11. The figure shows a timeline of Brownian motion periods and periods when the MTBD is attached to the microtubulin. Here, ff is the sampling period, $4/(2ni)$ is the minimal step duration and with kk can be influenced the detachment rate

For the Hoover-Holian oscillator, we set $HH = 1$, $PB = MKT = 0$ and similarly for the others oscillators. The projection of its attractor into the p-x plane is shown in Fig. 6.

Fig. 12 shows the situation for two domains (red and blue). When the movement time along the potential curve to its minimum is neglected, only the period L and the ratio rat (position of the minimum inside the period) are essential. The steps of both domains do not switch regularly. A more complicated situation is shown in Fig. 13. After the movement of the blue domain (4_1), the distance between both domains δ is relatively large. The red domain exhibits two steps $(2_2$ and 2_3, numbers 4 and 2 correspond to the different starting positions in the current instant). The critical distance δ is explainable as the stiffness measure between both domains.
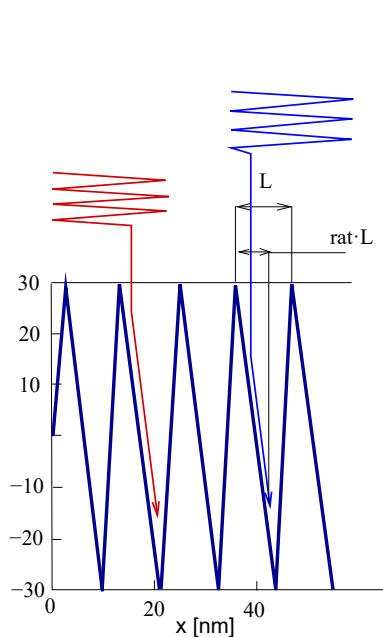

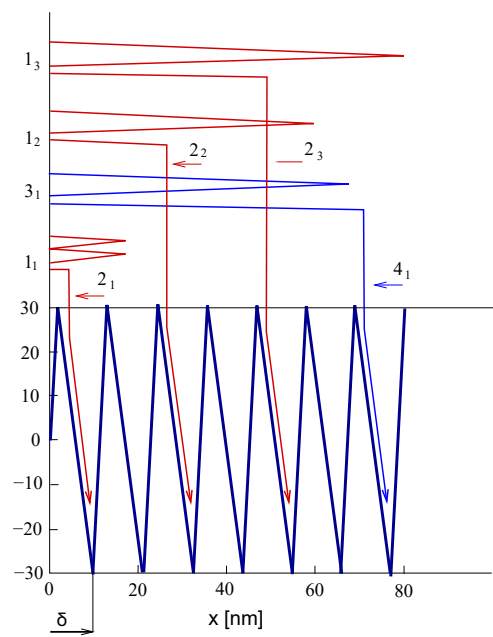Fig. 12. Illustration of a set of two Hoover-Holian oscillators

Fig. 13. Illustration of the movement further than one domain given by the Hoover-Holian oscillators

In Fig. 9, the centre of the attractor of the HH oscillator is at a point, where the potential has its minimum (last attachment point). The centre of the attractor moves by the value ps to respect the power stroke caused by the stalk priming. Under the action of external force $Fload$, the attached stalk deforms in the direction of this force in the amount $Fload \cdot invstif$. This deformation also causes the movement of the centre of the attractor.

The model needs changes to capture the catch bond effect. Parameter ni influences the time domain, parameter kk is changed, and parameters cb and $deltacb$ were introduced. The situation on the time axis is scratched in Figs. 11 and 14.
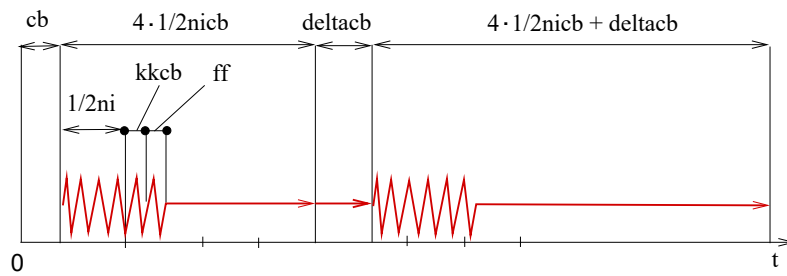

Fig. 14. Illustration of modelling the catch bond effect

4. Results and discussion

The first case studied in this work is with $Fload = 0$. Its results are shown in Fig. 15a. Three possible steps are visible there, as denoted by the three circles. In Fig. 15b, we can see the movement of the MTBDs over time. It is worth pointing out that these results are only qualitative. Further development is necessary to obtain physiological values.

Next, we studied the influence of the load. In Fig. 16a, steps for $Fload = -8$ are shown. The movement of the dynein is zero, finally. If we want to make the dynein move again, we must consider the catch bond effect starting for $Fload = -5$. It produces non-zero movement, as shown in Fig. 16b. The black line corresponds to the centre of dynein and the green line is the distance between both MTBDs.
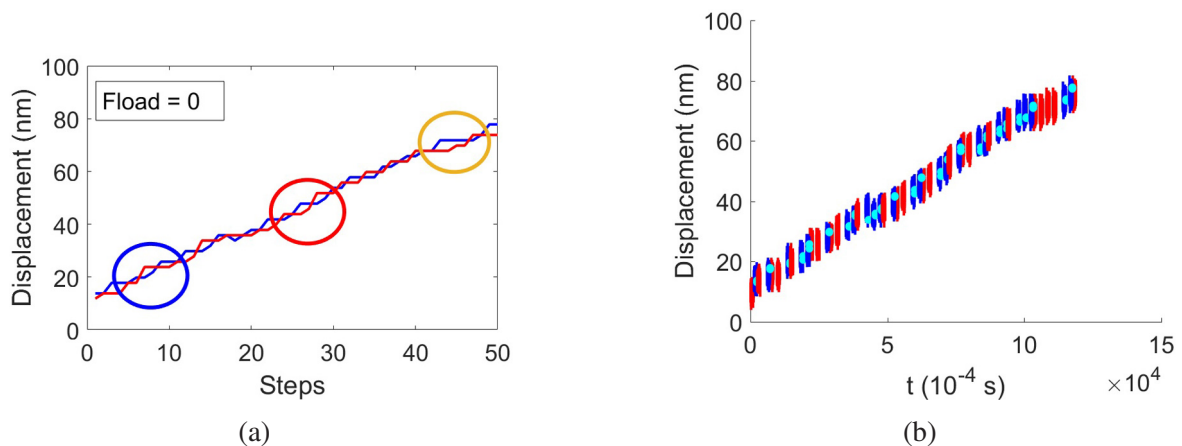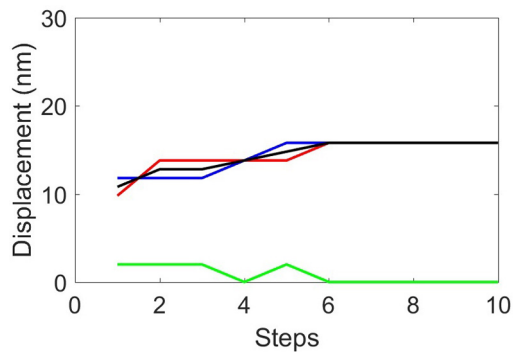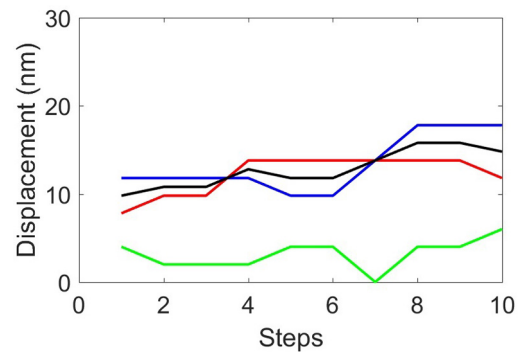

(a)

(b)

Fig. 15. Results of simulation with $Fload = 0$, which produces three possible kinds of steps: "inchworm" (blue circle), "hand-over-hand" (red circle), and non-alternate non-passing steps (orange circle)

(a) Without the catch bond effect, the higher load causes smaller steps than the case of $Fload = 0$ (red and blue – a position of both legs, green – a distance of legs)

(b) Inclusion of the catch bond effect helps the movement even for higher loads than usual (red and blue – a position of both legs, green – a distance of legs)

Fig. 16. Results of simulation with $Fload = -8$

Fig. 17 presents the results for the dependence between load and velocity. The red line corresponds with the catch bond effect starting with $Fload = 5$. These results are comparable with experimental results from [17], see Fig. 18. Due to the catch bond effect, the dynein slides even for $Fload > 5$ with a constant velocity.
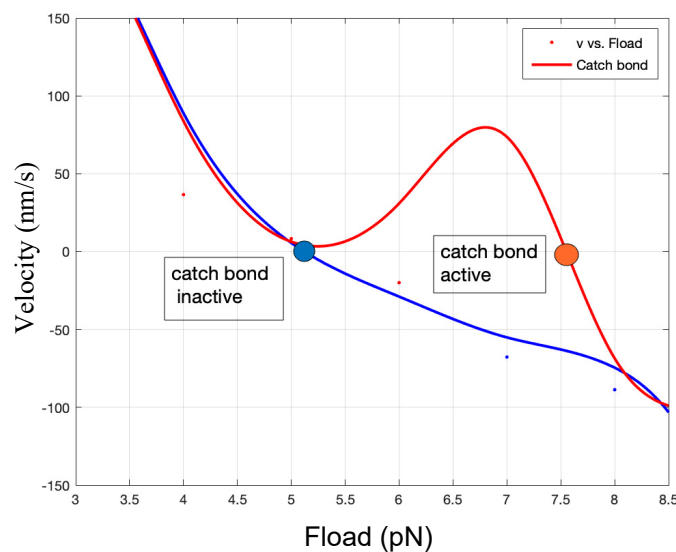

Fig. 17. Dependency between $Fload$ and the velocity

5. Conclusion

The described simple model presents the possibility of modelling the dynein movement by the Hover-Holian oscillator. These first results show that the model can produce all-important effects connected with dynein – its different steps movement, the catch bond effect, or velocity decrease with increasing load. In the future, we will focus on finding such coefficients for the model, which produces qualitative results and quantitative results.
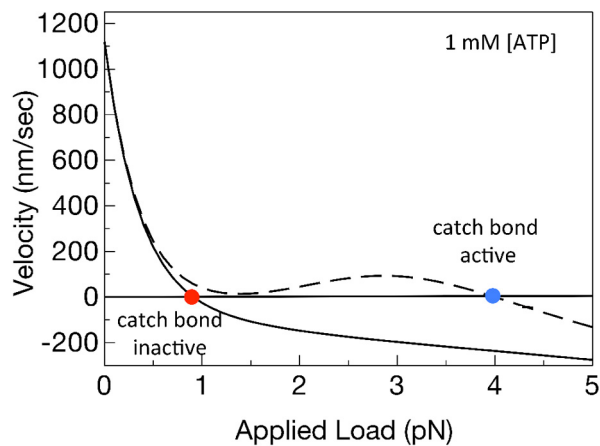
Fig. 18. Influence of catch bond effect, adapted from [17]

Acknowledgements

References

[1] Abraham, Z., Hawley, E., Hayosh, D., Webster-Wood, V. A., Akkus, O., Kinesin and dynein mechanics: Measurement methods and research applications, Journal of Biomechanical Engineering 140 (2018) 0208051–02080511. https://doi.org/10.1115/1.4037886

[2] Ait-Haddou, R., Herzog, W., Brownian ratchet models of molecular motors, Cell Biochemistry and Biophysics 38 (2003) 191–213. https://doi.org/10.1385/CBB:38:2:191

[3] Belyy, V., Hendel, N. L., Chien, A., Yildiz, A., Cytoplasmic dynein transports cargos via load-sharing between the heads, Nature Communications 5 (2014) No. 5544.
https://doi.org/10.1038/ncomms6544

[4] Bhabha, G., Johnson, G. T., Schroeder, C. M., Vale, R. D., How dynein moves along microtubules, Trends in Biochemical Sciences 41 (1) (2016) 94–105. https://doi.org/10.1016/j.tibs.2015.11.004

[5] Brenner, S., Berger, F., Rao, L., Nicholas, M. P., Gennerich, A., Force production of human cytoplasmic dynein is limited by its processivity, Science Advances 6 (15) (2020) No. eaaz4295.
https://doi.org/10.1126/sciadv.aaz4295

[6] Calkins, D. J., A neurorogical perspective on glaucoma, Glaucoma Today 2008 (2008) 18–20.

[7] Carter, A. P., Crystal clear insights into how the dynein motor moves, Journal of Cell Science 126 (2013) 705–713. https://doi.org/10.1242/jcs.120725

[8] Carter, A. P., Diamant, A. G., Urnavicius, L., How dynein and dynactin transport cargos: A structural perspective, Current Opinion in Structural Biology 37 (2016) 62–70.
https://doi.org/10.1016/j.sbi.2015.12.003

[9] Chen, X.-J., Xu, H., Cooper, H. M., Liu, Y., Cytoplasmic dynein: A key player in neurodegenerative and neurodevelopmental diseases, Science China Life Sciences 57 (4) (2014) 372–377.
https://doi.org/10.1007/s11427-014-4639-9

[10] Chen, J., Zhang, X., Lin, S., Wang, H., Gu, L., Multiscale modeling of skeletal muscle active contraction in relation to mechanochemical coupling of molecular motors, Micromachines 6 (7) (2015) 902–914. https://doi.org/10.3390/mi6070902

[11] Coronaviridae and the cytoskeleton, Cytoskeleton News (2020), http://www.cytoskeleton.com.

[12] Crossley, L., Garrett, C. A., Hafezparast, M., Madzvamuse, A., From the cell membrane to the nucleus: Unearthing transport mechanisms for dynein, Bulletin of Mathematical Biology 74 (9) 2012 2032–2061. https://doi.org/10.1007/s11538-012-9745-x

[13] Goedecke, D. M., Elston, T. C., A model for the oscillatory motion of single dynein molecules, Journal of Theoretical Biology 232 (2005) 27–39. https://doi.org/10.1016/j.jtbi.2004.07.017

[14] Han, Y.-R., Tong-Jun, Z., Yong, Z., Wei-Li, Y., Effective potential of a two-state model for molecular motor, Communications in Theoretical Physics 43 (2005) 377–381. https://doi.org/10.1088/0253-6102/43/2/035

[15] Hoover, W. G., Aoki, K., Hoover, C. G., De Groot, S. V., Time-reversible deterministic thermostats, Physica D: Nonlinear Phenomena 187 (1–4) (2004) 253–267. https://doi.org/10.1016/j.physd.2003.09.016

[16] Hoover, W. G., Hoover, C. G., Ergodicity of a time-reversibly thermostated harmonic oscillator and the 2014 Ian Snook Prize, Computational Methods in Science and Technology 20 (3) (2014) 87–92. https://doi.org/10.12921/cmst.2014.20.03.87-92

[17] Johnson, C. M., Investigating the slow axonal transport of neurofilaments: A precursor for optimal neuronal signaling, Ph.D. thesis, Ohio University, Athens, United States of America, 2016.

[18] Kunwar, A., Tripathy, S. K., Xu, J., Gross, S. P., Mechanical stochastic tug-of-war models cannot explain bidirectional lipid-droplet transport, Proceedings of the National Academy of Sciences of the United States of America 108 (47) (2011) 18960–18965. https://doi.org/10.1073/pnas.1107841108

[19] Li, L., Alper, J., Alexov, E., Cytoplasmic dynein binding, run length, and velocity are guided by long-range electrostatic interactions, Scientific Reports 6 (2016) No. 31523. https://doi.org/10.1038/srep31523

[20] Nair, A., Chandel, S., Mitra, M. K., Muhuri, S., Chaudhuri, A., Catch bond mechanism in dynein motor driven collective transport, 2016, arXiv:1602.02423v1. https://doi.org/10.48550/arXiv.1602.02423

[21] Nandi, R., Täuber, U. C., Priyanka, Dynein-inspired multilane exclusion process with open boundary conditions, Entropy 23 (10) (2021) No. 1343. https://doi.org/10.3390/e23101343

[22] Parmeggiani, A., Jülicher, F., Ajdari, A., Prost, J., Energy transduction of isothermal ratchets: Generic aspects and specific examples close to and far from equilibrium, Physical Review E 60 (2) (1999) 2127–2140. https://doi.org/10.1103/PhysRevE.60.2127

[23] Posch, H. A., Hoover, W. G., Vesely, F. J., Canonical dynamics of the Nosé oscillator: Stability, order, and chaos, Physical review A 33 (6) (1986) 4253–4265. https://doi.org/10.1103/PhysRevA.33.4253

[24] Puri, P., Gupta, N., Chandel, S., Naskar, S., Nair, A., Chaudhuri, A., Mitra, M. K., Muhuri, S., Dynein catch bond as a mediator of codependent bidirectional cellular transport, Physical Review Research 1 (2019) No. 023019. https://doi.org/10.1103/PhysRevResearch.1.023019

[25] Qiu, W., Derr, N. D., Goodman, B. S., Villa, E., Wu, D., Shih, W., Reck-Peterson, S. L., Dynein achieves processive motion using both stochastic and coordinated stepping, Nature Structural & Molecular Biology 19 (2) (2012) 193–200. https://doi.org/10.1038/nsmb.2205

[26] Rai, A. K., Rai, A., Ramaiya, A. J., Jha, R., Mallik, R., Molecular adaptations allow dynein to generate large collective forces inside cells, Cell 152 (2019) 172–182. https://doi.org/10.1016/j.cell.2012.11.044

[27] Reck-Peterson, S. L., Yildiz, A., Carter, A. P., Gennerich, A., Zhang, N., Vale, R. D., Single-molecule analysis of dynein processivity and stepping behavior, Cell 126 (2006) 335–348. https://doi.org/10.1016/j.cell.2006.05.046

[28] Roberts, A. J., Kon, T., Knight, P. J., Sutoh, K., Burgess, S. A., Functions and mechanics of dynein motor proteins, Nature Reviews Molecular Cell Biology 14 (11) (2013) 713–726. https://doi.org/10.1038/nrm3667

[29] Scherer, J., Yi, J., Vallee, R. B., Role of cytoplasmic dynein and kinesins in adenovirus, FEBS Letters 594 (12) (2020) 1838–1847. https://doi.org/10.1002/1873-3468.13777

[30] Toba, S., Watanabe, T. M., Yamaguchi-Okimoto, L., Higuchi, H., Overlapping hand-over-hand mechanism of single molecular motility of cytoplasmic dynein, Proceedings of the National Academy of Sciences of the United States of America 103 (15) (2006) 5741–5745. https://doi.org/10.1073/pnas.0508511103

[31] Trott, L., A physical model describing the transport mechanisms of cytoplasmic dynein, Ph.D. thesis, University of Sussex, Sussex, 2016.

[32] Trott, L., Hafezparast, M., Madzvamuse, A., A mathematical understanding of how cytoplasmic dynein walks on microtubules, Royal Society Open Science 5 (2018) No. 171568. https://doi.org/10.1098/rsos.171568

[33] Wilke, P., Reithmann, E., Frey, E., Two-species active transport along cylindrical biofilaments is limited by emergent topological hindrance, Physical Review X 8 (2018) No. 031063. https://doi.org/10.1103/PhysRevX.8.031063

[34] Wolf, A., Determining Lyapunov exponents from a time series, Physica D 16 (1985) 285–317. https://doi.org/10.1016/0167-2789(85)90011-9

[35] Zhao, X. Y., Sun, W., Zhang, J. P., Tala, Guo, W. S., A model for the coordinated stepping of cytoplasmic dynein, Biochemical and Biophysical Research Communications 453 (4) (2014) 686–691. https://doi.org/10.1016/j.bbrc.2014.09.138